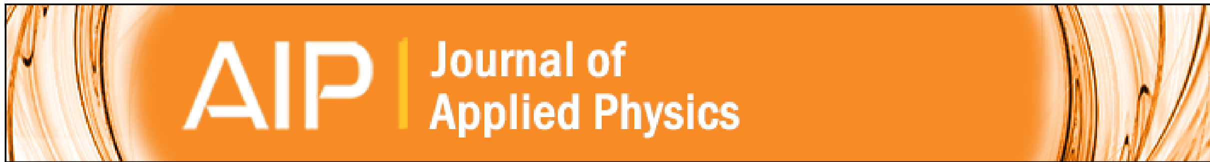

Effect of metal-ion doping on the optical properties of nanocrystalline ZnO thin films

A. Mendoza-Galván, C. Trejo-Cruz, J. Lee, D. Bhattacharyya, J. Metson, P. J. Evans, and U. Pal

Citation: Journal of Applied Physics 99, 014306 (2006); doi: 10.1063/1.2158503
View online: http://dx.doi.org/10.1063/1.2158503
View Table of Contents: http://scitation.aip.org/content/aip/journal/jap/99/1?ver=pdfcov
Published by the AIP Publishing

Re-register for Table of Content Alerts

Create a profile.

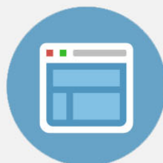

Sign up today!

[This article is copyrighted as indicated in the article. Reuse of AIP content is subject to the terms at: http://scitation.aip.org/termsconditions. Downloaded to] IP: 148.228.150.246 On: Tue, 07 Jan 2014 22:12:07

Effect of metal-ion doping on the optical properties of nanocrystalline ZnO thin films

A. Mendoza-Galván and C. Trejo-Cruz
CINVESTAV-IPN, Unidad Querétaro, Apartado Postal 1-798, Querétaro, Querétaro 76001, Mexico

J. Lee and D. Bhattacharyya
Department of Mechanical Engineering, The University of Auckland, Private Bag 92019, Auckland, New Zealand

J. Metson
Department of Chemistry, The University of Auckland, Private Bag 92019, Auckland, New Zealand

P. J. Evans
Australian Nuclear Science and Technology Organization, PMB 1, Menai, NSW 2234, Australia

U. Pal[a)]
Instituto de Física, Universidad Autónoma de Puebla, Apartado Postal J-48, Puebla, Puebla 72570, Mexico

(Received 2 August 2005; accepted 14 November 2005; published online 10 January 2006)

Optical properties of metal (Al, Ag, Sb, and Sn)-ion-implanted ZnO films have been studied by ultraviolet-visible spectroscopy and spectroscopic ellipsometric techniques. The effects of metal-ion doping on the optical band gap (E_g), refractive index (n), and extinction coefficient (k) of nanocrystalline ZnO films have been studied for the similar implantation dose of all the metal ions. The ellipsometric spectra of the ion-implanted samples could be well described by considering an air/roughness/ZnO$-M$ (layer 1)/ZnO (layer 2)/glass model. The band gap of ZnO films increases with Al ion doping and decreases with doping of Ag, Sb, and Sn ions. The refractive index of ZnO films in the visible spectral region increases substantially on Sb and Sn ion doping, while it decreases to some extent with Al ion doping. © *2006 American Institute of Physics*.
[DOI: 10.1063/1.2158503]

I. INTRODUCTION

With a wide direct band gap (3.37 eV at room temperature) and high exciton binding energy (60 meV), ZnO is one of the most promising oxide semiconductors with applications in light-emitting devices,[1,2] window materials in solar cells, display devices,[3,4] high-temperature, high-power transistors,[5] and gas sensing.[6,7] Its piezoelectric properties are being explored for fabricating various pressure transducers and acoustic wave and optoacoustic devices.[8,9] However, the possibility of practical application of any semiconductor lies on the effective manipulation of its physical properties. An effective method for manipulating the physical properties of semiconductors involves impurity doping. Considerable work has been reported on the doping of ZnO with several dopants to tailor its electrical and optical properties. While the doping of different metals was successful for controlling the electrical properties of ZnO in thin films[10–12] and bulk forms[13,14] and has been widely reported, there are no reports of systematic studies of the optical properties of metal-doped ZnO, either in bulk or in thin-film forms.[15,16]

In the present work, we report on the optical properties of ZnO thin films doped with Al, Ag, Sb, and Sn by low-energy ion implantation. Utilizing ultraviolet-visible (UV-Vis) optical absorption and spectroscopic ellipsometry techniques, the optical constants of the ZnO thin films doped with different metals of similar contents were determined. The effects of metal-ion implantation on the morphology and crystallinity of the ZnO films have been studied by scanning electron microscopy (SEM) and x-ray-diffraction (XRD) techniques.

II. EXPERIMENT

ZnO thin films were deposited by radio frequency (rf) magnetron sputtering on microscopic glass substrates at room temperature. A ZnO target (99.9%) of 150 mm diameter was sputtered at 20 mTorr argon pressure and 250 W rf power for 40 min at a substrate to a target distance of 13 cm. The substrates were biased with -50 V during deposition. The thickness of the ZnO films was measured with an alpha-step profilometer. Ion implantation was carried out by using a metal vapor vacuum arc (MEVVA) ion source, a high-current device, which can readily produce ion-beam currents of several hundreds of milliampere on target. Using Ag, Al, Sn, and Sb (>99.9% purity) rods as targets, the implantation of metal ions into ZnO films were performed after 2000 conditioning shots at the chamber base pressure of 2×10^{-6} mbars and extraction potential of 40 kV. Using a 40 mA beam current, the metal ions of about 1.0×10^{16} cm^{-2} nominal dose were implanted. A Philips XL-30S scanning electron microscope (SEM) was used for the morphological observations of the planer and cross-sectional

[a)]Author to whom correspondence should be addressed; FAX: +52-222-2295611; electronic mail: upal@sirio.ifuap.buap.mx

 © 2006 American Institute of Physics

[This article is copyrighted as indicated in the article. Reuse of AIP content is subject to the terms at: http://scitation.aip.org/termsconditions. Downloaded to] IP: 148.228.150.246 On: Tue, 07 Jan 2014 22:12:07

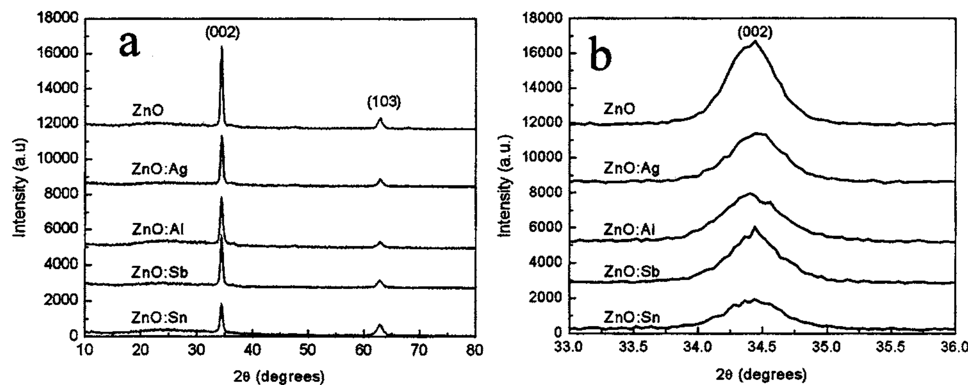

FIG. 1. (a) XRD patterns of the undoped and ion-implanted ZnO films; (b) a close view of the (002) diffraction peak of the doped and undoped ZnO films showing the variation of peak intensity and line broadening on metal-ion doping.

views of the implanted and unimplanted samples after gold coating over them. XRD studies were performed using a Rigaku/Dmax-2100 x-ray diffractometer equipped with a Cu anode (Cu $K\alpha$=0.154 06 nm). Depth profiling of each sample was carried out using a dynamic secondary-ion-mass spectrometry (SIMS) (CAMECA ims-5f) with $^{133}Cs^+$ as the primary ion, with a net accelerating voltage of 2.2 kV and a beam current of 15 nA. A 10 μm diameter area of the samples was analyzed from the center of a 250×250 μm^2 area rastered by the primary ions. To achieve the low incident energy and minimize matrix effects, secondary ions were collected as the MCs^+ species.[17]

Spectroscopic ellipsometry (SE) measurements were carried out with a Jobin Yvon Uvisel DH10 system in the spectral range of 1.5 – 5.0 eV. In order to eliminate light reflection from the back side of the substrate, this side was sandblasted prior to the SE measurements. For each sample, data were acquired at three angles of incidence; ϕ=60°, 65°, and 70°. Also, the reflectance (R) and transmittance (T) measurements at normal incidence were carried out with a FilmTek 3000 Scientific Computing International Inc. (SCI) thin-film metrology system in the range of 300–830 nm.

III. RESULTS AND DISCUSSION

A. Structure, morphology, and composition

XRD spectra of all the doped and undoped films (Fig. 1) revealed an intense (002) and weak (103) diffraction peaks of wurtzite phase ZnO, indicating that the films were highly oriented along the c axis. While the surface morphology of the samples (Fig. 2) revealed the formation of nanometer-size grains, their cross-sectional views revealed the formation of columnar structures. To monitor the effect of ion implantation on the crystallinity of the films, the intensity of the (002) diffraction peak was monitored. The intensity of the (002) diffraction peak decreased and its full width at half maximum (FWHM) increased on implanting the metal ions (see Table I), indicating a decrease in crystallinity of the samples. Such a decrease in crystallinity on ion implantation might be the result of metal-ion doping or ion-beam-induced damage produced during implantation. Though both the effects can contribute to the decreased crystallinity of the samples, from the cross-sectional SEM images of the doped samples, we could not detect any significant change in their morphology except some breaking of columnar grains of undoped ZnO films on implantation. In fact, such a reduction of crystallinity on doping of metals/semiconductors has been observed even in sputter-deposited composite films.[18,19] The reduction of crystallinity in the samples was further monitored by measuring the average particle size in the samples from the (002) diffraction peaks using the Scherrer formula:

$$P = (K\lambda)/\beta \cos \theta, \qquad (1)$$

where P is the average crystallite size, λ is the wavelength of the x ray (λ=1.5406 Å), θ is the diffraction angle, β is the FWHM, and K is a constant of proportionality usually taken as equal to unity. The average particle size obtained for the samples are presented in Table I. The average particle size of ZnO decreased on metal-ion doping. The ionic radius of Zn and doped elements in the wurtzite ZnO crystals are expected to be $r(Zn^{+2})$=74 pm, $r(Ag^{+1})$=126 pm, $r(Al^{+3})$=50 pm, $r(Sb^{+5})$=63 pm, and $r(Sn^{+4})$=69 pm. Therefore, a maximum lattice deformation is expected for Al doping due to its biggest ionic radius. However, either from the cross-sectional SEM images or from the values obtained through the Scherrer formula (Table I), we could not detect any systematic change in the average particle size for the doped samples, which indicates that the lattice deformation or the size of the crystallites depends not only on the ionic radius of the doped elements but also on their charge distributions.

SIMS depth profile analysis of the samples revealed different depths of penetration for different metal ions. While

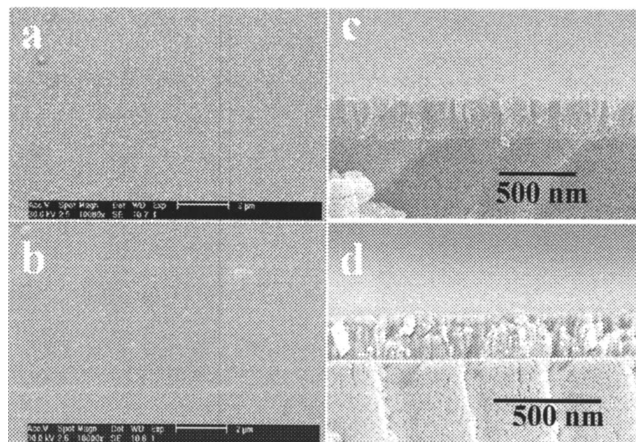

FIG. 2. Typical surface [(a) and (b)] and cross-sectional morphology [(c) and (d)] of the pure and Al-implanted ZnO samples, respectively. While (a) and (c) correspond to the surface and cross-sectional SEM images of the pure ZnO, the micrographs (b) and (d) correspond to the corresponding micrographs of Al-implanted ZnO films.

[This article is copyrighted as indicated in the article. Reuse of AIP content is subject to the terms at: http://scitation.aip.org/termsconditions. Downloaded to] IP: 148.228.150.246 On: Tue, 07 Jan 2014 22:12:07

TABLE I. Parameters obtained for the (002) diffraction lines and calculated particle size values.

Sample	2θ (degrees)	FWHM (degrees)	Integrated area	Average particle size, P (nm)
ZnO	34.412	0.4528	2437	20.4
ZnO:Ag	34.449	0.5001	1617	18.5
ZnO:Al	34.413	0.5767	1755	16.0
ZnO:Sb	34.437	0.4933	1590	18.7
ZnO:Sn	34.432	0.5374	1145	17.2

the Al ions penetrated most, the larger Sb ions penetrated the least depth. The depth profiles for metal ions in the samples are presented in Fig. 3. The penetration depth for each of the ions in the films is listed in Table II.

B. Optical properties

The SE measurements provide the change in the polarization state that an incident light beam with a known polarization state suffers when it is reflected by a surface. This change is expressed as the ratio between the complex reflection coefficients for polarization parallel r_p and perpendicular r_s to the plane of incidence,[20]

$$\rho = \frac{r_p}{r_s} = \tan \Psi \exp(i\Delta). \qquad (2)$$

As shown in Eq. (1), the spectroscopic measurements are expressed in terms of the ellipsometric angles Ψ and Δ as the functions of the photon energy. Thus, the construction of a physical model for the coefficients r_p and r_s allows the determination of several parameters by fitting the calculated spectra using Eq. (2) with the experimental spectra. In particular, the optical constants, refractive index (n), extinction coefficient (k), and thicknesses of unknown layers can be obtained. In the case of anisotropic films, Eq. (2) makes sense only if the principal axes are in the plane of incidence.[20] This requirement is fulfilled in the present case, as our x-ray data revealed that the crystallographic c axis is highly oriented perpendicular to the sample surface.[21] Thus, the ZnO dielectric function has two components: one parallel ($\varepsilon_{\parallel}$) and another perpendicular ($\varepsilon_{\perp}$) to the c axis.[22] However, it has been pointed out that for this configuration (c axis perpendicular to the sample surface), the $\varepsilon_{\parallel}$ component contributes relatively little to the SE measurements.[23] Therefore, the analysis is carried out considering the films as isotropic, i.e., with an *effective* optical response.

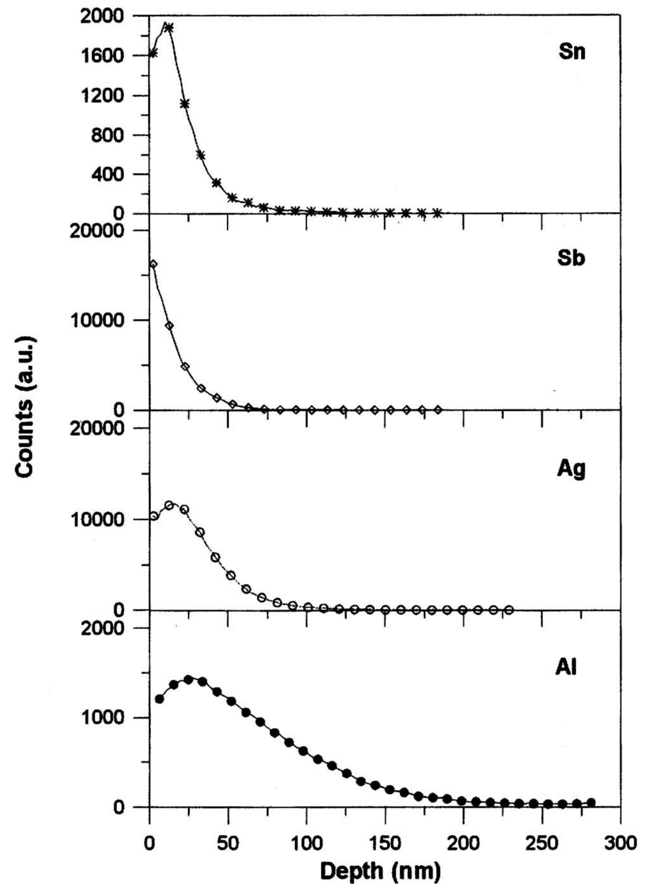

FIG. 3. SIMS depth profiles of the metal-ion-implanted ZnO films.

Figure 4 shows the experimental and best-fit ellipsometric spectra for the measurements taken at the three angles of incidence on the undoped ZnO sample. The symbols correspond to experimental data and the lines to the best-fit ellipsometric spectra. It can be noted in Fig. 4 that for all the angles of incidence, psi and delta spectra show interference oscillations for photon energies lower than about 3.3 eV, which corresponds to the band-gap energy of ZnO.

The best-fit calculated spectra (Fig. 4) were obtained, considering an air/roughness/ZnO/glass system, where the surface roughness was modeled with Bruggeman's effective medium approximation,[20] comprised of a mixture of 50%-50% volume fractions for air and ZnO [see Fig. 5(a)]. The

TABLE II. Surface roughness (r), thickness of the metal-doped (t_1) and undoped (t_2) ZnO layers, and effective band-gap values for the samples obtained from best-fit ellipsometric spectra. The t_1 values estimated from the SIMS depth profiles of the samples are included for comparison.

Sample	r (nm)	t_1 (nm)	t_2 (nm)	t_1 (nm) estimated from SIMS depth profiles	E_g (eV)
ZnO	15.5	⋯	277	0.0	3.33
ZnO–Ag	7.9	51	197	75	3.13
ZnO–Al	14.1	136	131	170	3.45
ZnO–Sb	9.8	41	203	50	2.99
ZnO–Sn	18	45	240	70	3.31

[This article is copyrighted as indicated in the article. Reuse of AIP content is subject to the terms at: http://scitation.aip.org/termsconditions. Downloaded to] IP: 148.228.150.246 On: Tue, 07 Jan 2014 22:12:07

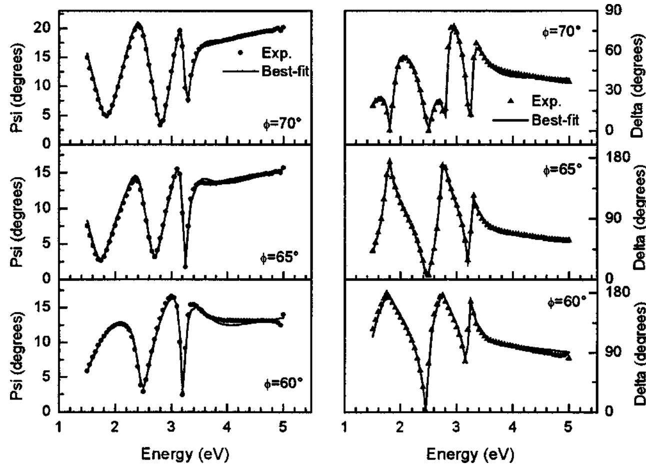

FIG. 4. Ellipsometric spectra for the undoped ZnO film for different angles of incidence.

effective dielectric function of the undoped ZnO film was represented by a generalized form of the Lorentz harmonic oscillator expression, patented by SCI, which is consistent with the Kramers-Kroning relationship.[24] In this case, the optical constants of ZnO were represented, considering the parameters of two oscillators. The fitting was performed using simultaneously the measurements at the three angles of incidence. The optimum values of film thickness and roughness producing the best fit for the experimental spectra are listed in Table II, while the optical constants obtained for the films are discussed below.

In Fig. 6, the ellipsometric spectra of metal-doped ZnO samples obtained for an incident angle of 65° are presented. There are noticeable differences between the SE data of the metal-doped (Fig. 6) and undoped samples (Fig. 4) for $\phi = 65°$. The differences are most apparent for the samples implanted with Ag, Sb, and Sn metal ions, where the interference oscillations revealed by the undoped sample are strongly damped. For instance, the delta spectrum for the ZnO sample shows a sharp deep minimum and a sharp high maximum in the 2–3 eV spectral range; while the delta spectrum of the ZnO–Sb sample shows broad and less intense features in the same spectral range. A similar behavior can be observed in the spectra of the other metal-implanted samples. The latter indicates that the metal-implanted samples have a different optical response.

Considering the points mentioned in the previous paragraph and taking into account that the implanted metal ions

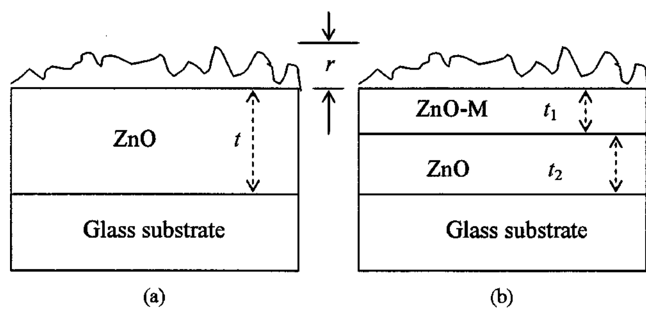

FIG. 5. Layered models used to analyze the ellipsometric spectra: (a) for the un-doped ZnO sample; (b) for metal-doped ZnO samples.

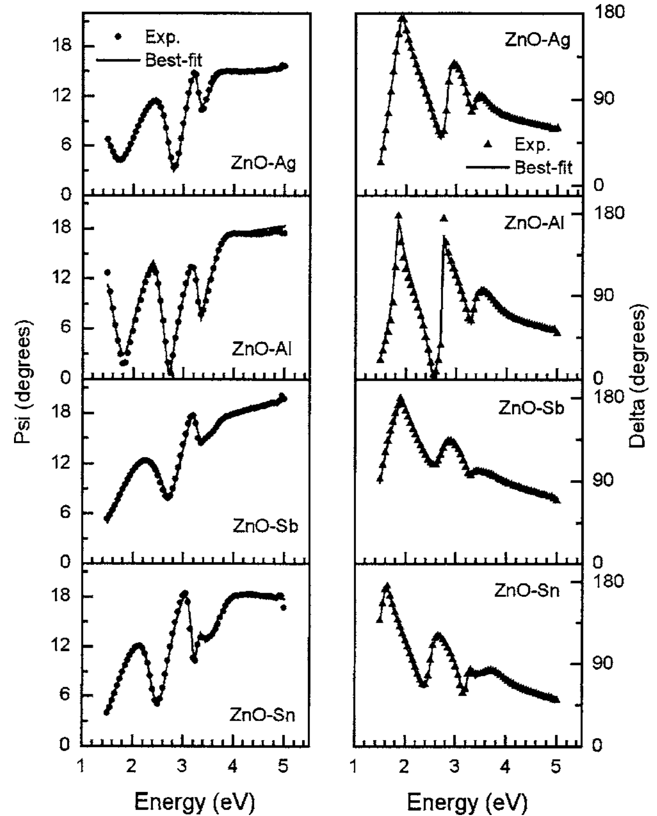

FIG. 6. Ellipsometric spectra of metal-doped ZnO samples for 65° incidence angle.

did not penetrate throughout the film thickness (as revealed from the SIMS profiles in Fig. 3), the optical system considered to describe the SE data in Fig. 6 comprised of two layers and a characteristic surface roughness, i.e., an air/roughness/ZnO$-M$ (layer 1)/ZnO (layer 2)/glass system, which is represented schematically in Fig. 5(b). In this model, the layer underneath the surface corresponds to the metal-implanted region, and the second layer corresponds to an undoped ZnO material. The unknown parameters for this model are the optical constants of the ZnO$-M$ layer, the roughness value (r), and the thicknesses t_1 and t_2 of the doped and undoped layers, respectively. For layer 2, the optical constants were those obtained from the fitting of the SE data in Fig. 4. The effective dielectric function for the ZnO$-M$ layer was represented again by the generalized Lorentz expression as described earlier. For these samples, the fitting was carried out considering simultaneously the SE measurements at the three angles of incidence, obtaining similar results to those shown in Fig. 6. The values obtained for the best-fit unknown parameters (r, t_1, and t_2) are presented in Table II.

In spite of the simplicity of the model considered to analyze the SE results, it can be noted that all the features in the experimental spectra (Fig. 6) are adequately described. Furthermore, the values obtained for the thicknesses of the ZnO$-M$ layers (t_1) presented in Table II agree well with the trend of the maximum penetration depth of the metal ions obtained from SIMS depth profiles (Fig. 3).

The effective optical constants, refractive index (n), and extinction coefficient (k), for the undoped and doped ZnO

[This article is copyrighted as indicated in the article. Reuse of AIP content is subject to the terms at: http://scitation.aip.org/termsconditions. Downloaded to] IP: 148.228.150.246 On: Tue, 07 Jan 2014 22:12:07

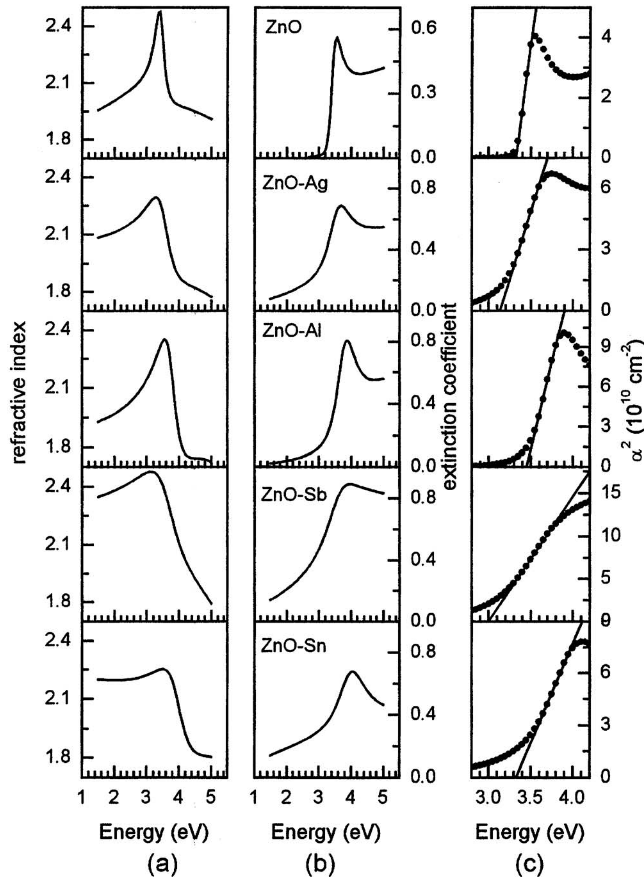

FIG. 7. (a) Refractive index and (b) extinction coefficient spectra for the undoped and metal-doped ZnO samples. (c) α^2 vs photon energy plots of the corresponding samples used to determine their optical band gaps.

films obtained from the analyses of the SE spectra are shown in Fig. 7. The n and k spectra for the ZnO films show good agreement with data previously reported for single crystals and thin films.[22,25] In particular, sharp maxima in n and k around the band-gap energy are clearly seen and are associated with excitonic-like transitions.[22,25] For the ZnO–M layers, the optical constants show broad maxima around the band gap, but at different photon energy values. The broadness could be associated with some degree of amorphization of the ZnO matrix in the metal-implanted layers. In fact, the integrated area below the (002) diffraction line (Table I), which could be considered as a measure of crystallinity, decreased for doped samples, and the effect is most pronounced for the Sn-doped sample.

From the k spectra in Fig. 7(b), the absorption coefficient $\alpha = 4\pi k/\lambda$ (λ=wavelength) was calculated, and plotting α^2 vs E, the optical band gap (E_g) was obtained by fitting the linear portion for each spectrum, as shown in Fig. 7(c). The E_g values obtained in this way are listed in Table II. For the undoped sample, the E_g value of 3.33 eV agrees well with reported literature values. The optical band gaps for the ZnO–M layers are 3.13, 3.45, 2.99, and 3.31 eV for M =Ag, Al, Sb, and Sn, respectively. Clearly, there is an increasing redshift in the band gap for the implantation of Sn, Ag, and Sb ions, respectively, and a blueshift for the Al ions. Such a redshift of the optical band gap in sputter-deposited Ag-doped ZnO films has been reported by Jeong *et al.*[15] Also, a gradual blueshift of the band gap and the degradation of crystallinity with increasing Al content in sputter-deposited ZnO films is reported.[26] It must be noticed that the refractive index of ZnO films in the visible spectral range increases on Sb and Sn doping.

In Fig. 8 the reflectance (R) and transmittance (T) spectra of the samples measured at normal incidence are presented. It can be noticed that T for the undoped ZnO film is very high (about 90%). On metal-ion implantation, the R and T spectra are drastically modified. However, the occurrence of interference oscillations in these spectra indicates good optical quality of the materials. The transmittance of the implanted ZnO films decreased gradually for Al, Ag, Sn, and Sb doping, attaining a value of about 60% for Sb doping. Such a decrease in optical transmittance has also been observed in Ag-doped ZnO sputtered films by Jeong *et al.*[15] On the other hand, the maxima of the R spectra attain higher values in the

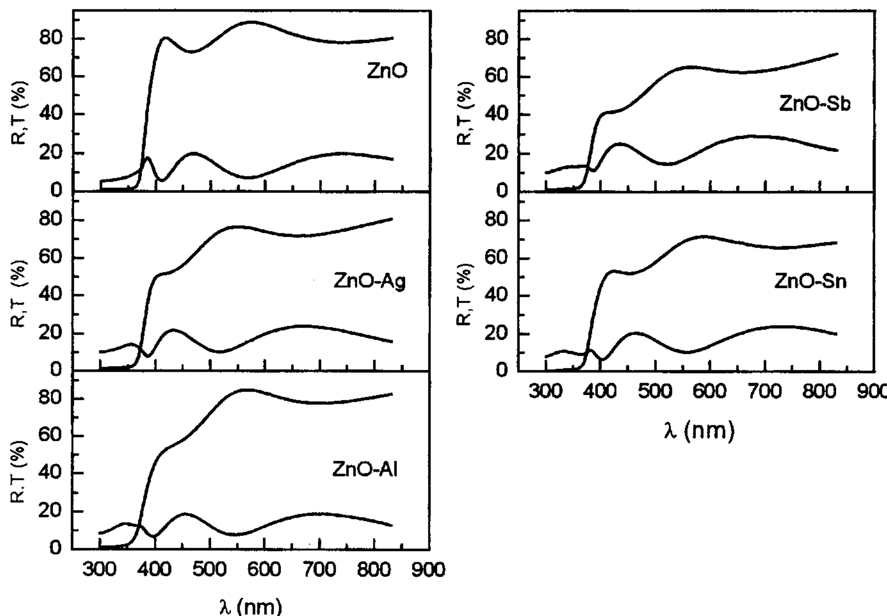

FIG. 8. Reflectance and transmittance spectra of ZnO samples.

[This article is copyrighted as indicated in the article. Reuse of AIP content is subject to the terms at: http://scitation.aip.org/termsconditions. Downloaded to] IP: 148.228.150.246 On: Tue, 07 Jan 2014 22:12:07

long-wavelength range in the same order as T decreases. This latter result is related with the fact that for low photon energies the refractive index decreases for Sb, Sn, Ag, and Al doping, as can be noticed in Fig. 7(a). Thus, the effective optical constants obtained from the SE analyses give a good description of the linear optical response of the ion-implanted ZnO films studied here.

IV. CONCLUSIONS

Optical properties of nanocrystalline ZnO thin films doped with Al, Ag, Sb, and Sn by low-energy ion implantation are determined by spectroscopic ellipsometry. Considering a simple air/roughness/ZnO–M (layer 1)/ZnO (layer 2)/glass model for the doped films and utilizing a generalized form of the Lorentz harmonic oscillator expression for effective dielectric function of ZnO, all the features in the ellipsometric spectra of the films could be well described. Apart from affecting the crystallinity of the ZnO films, implantation of the metal ions strongly affects their band gap, the refractive index in the visible region, and the extinction coefficients.

ACKNOWLEDGMENTS

This work is supported by the CONACyT, Mexico (Grant No. 46269) and the Australian Institute of Nuclear Science and Engineering (AINSTU0603). We acknowledge the assistance of Dr. Z. Li, Dr. K. Prince, C. Depagne, and D. Button and the facilities extended by the Research Center for Surface and Materials Science, the University of Auckland.

[1] K. Minegishi, Y. Koiwai, Y. Kikuchi, and K. Yano, Jpn. J. Appl. Phys., Part 2 **36**, L1453 (1997).
[2] D. C. Look, Mater. Sci. Eng., B **80**, 383 (2001).
[3] K. L. Chopra, S. Major, and D. K. Pandya, Thin Solid Films **102**, 1 (1983).
[4] G. A. Emelchenko, A. N. Gruzinsev, V. V. Masalov, E. N. Samarov, A. V. Bazhenov, and E. E. Yakimov, J. Opt. A, Pure Appl. Opt. **7**, S213 (2005).
[5] W. Gao, Z. Li, R. Harikisun, and S.-S. Chang, Mater. Lett. **57**, 1435 (2003).
[6] E. Comini, G. Faglia, G. Sberveglieri, Z. Pan, and Z. L. Wang, Appl. Phys. Lett. **81**, 1869 (2002).
[7] J. F. Chang, H. H. Kuo, I. C. Leu, and M. H. Hon, Sens. Actuators B **84**, 258 (2002).
[8] Y. Yoshino, T. Makino, Y. Katayama, and T. Hata, Vacuum **59**, 538 (2000).
[9] J. B. Lee, H. J. Kim, S. G. Kim, C. S. Hwang, S.-H. Hong, Y. H. Shin, and N. H. Lee, Thin Solid Films **435**, 179 (2003).
[10] S. Bose, S. Ray, and A. K. Barua, J. Phys. D **29**, 1873 (1996).
[11] W. W. Wenas, A. Yamada, K. Takahashi, M. Yoshino, and M. Konagai, J. Appl. Phys. **70**, 7119 (1991).
[12] S. B. Qadri, H. Kim, J. S. Horwitz, and D. B. Chrisey, J. Appl. Phys. **88**, 6564 (2000).
[13] H. Czternastek, Opto-Electron. Rev. **12**, 49 (2004).
[14] J. J. Robbins, J. Harvey, J. Leaf, C. Fry, and C. A. Wolden, Thin Solid Films **473**, 35 (2005).
[15] S. H. Jeong, B. N. Park, S. B. Lee, and J.-H. Boo, Surf. Coat. Technol. **193**, 340 (2005).
[16] N. R. Aghamalyan, E. A. Kafadaryan, R. K. Housepyan, and S. I. Petrosyan, Semicond. Sci. Technol. **20**, 80 (2005).
[17] J. B. Metson and K. E. Prince, Surf. Interface Anal. **28** 159 (1999).
[18] O. Vazquez-Cuchillo, U. Pal, and C. Vazquez-Lopez, Sol. Energy Mater. Sol. Cells **70**, 369 (2001).
[19] U. Pal, N. Koshizaki, S. Terauchi, and T. Sasaki, Microsc. Microanal. Microstruct. **8**, 403 (1997).
[20] G. E. Jellison, Jr., Thin Solid Films **234**, 416 (1993).
[21] R. M. A. Azzam and N. M. Bashara, *Ellipsometry and Polarized Light* (North Holland, Amsterdam, 1977), Chap. 4.
[22] D. M. Kolb and H.-J. Schulz, in *Current Topics in Materials Science*, edited by E. Koldis (North-Holland, Amsterdam, 1981), Vol. 7, p. 226.
[23] D. E. Aspnes, J. Opt. Soc. Am. **70**, 1275 (1980).
[24] E. Zawaideh, U.S. Patent No. 5889592 (1999).
[25] P. L. Washington, H. C. Ong, J. Y. Da, and R. P. H. Chang, Appl. Phys. Lett. **72**, 3261 (1998).
[26] S. H. Jeong, J. W. Lee, S. B. Lee, and J.-H. Boo, Thin Solid Films **435**, 78 (2003).

[This article is copyrighted as indicated in the article. Reuse of AIP content is subject to the terms at: http://scitation.aip.org/termsconditions. Downloaded to] IP: 148.228.150.246 On: Tue, 07 Jan 2014 22:12:07